

Electroweak baryogenesis and electron EDM in the TNMSSM

Xiang Yang^{1,2,3*}, Ming-Hui Guo^{1,2}, Jin-Lei Yang^{1,2,3†}, Qing-Hua Li^{1,2,3‡}, Tai-Fu Feng^{1,2,3,4§}

¹ *Department of Physics, Hebei University, Baoding 071002, China*

² *Hebei Key Laboratory of High-precision Computation and Application of Quantum Field Theory, Baoding, 071002, China*

³ *Hebei Research Center of the Basic Discipline for Computational Physics, Baoding, 071002, China and*

⁴ *Department of Physics, Chongqing University, Chongqing 401331, China*

(Dated: February 18, 2025)

Abstract

We have studied the impact of CP-violating (CPV) effects on electroweak baryogenesis (EWBG) and the electric dipole moment (EDM) of electron (d_e), the electric dipole moment (EDM) of mercury neutron (d_n) and the electric dipole moment (EDM) of (d_{Hg}) in an extension of the Minimal Supersymmetric Standard Model (MSSM). The model incorporating a $SU(2)$ triplet with hypercharges of ± 1 and a gauge singlet from the standard model that is mutually coupled, is collectively referred to as the next-to-minimal supersymmetric standard model with triplets (TNMSSM). Furthermore, we discuss the strong first-order phase transition (PT) achieved by this model via tree-level effects. The numerical results indicate that the TNMSSM can account for the observed baryon asymmetry. Additionally, the regions favored by EWBG can be compatible with the corresponding electron EDM bounds when different contributions to the d_e cancel each other out.

PACS numbers:

Keywords: EWBG, EDM, TNMSSM

* yangxiang202406@163.com

† jlyang@hbu.edu.cn

‡ lqhlqh202408.163.com

§ fengtf@hbu.edu.cn

I. INTRODUCTION

Although the standard model (SM) has been experimentally confirmed in many theoretical predictions, there still exist phenomena that cannot be explained by the SM. One of the most intriguing issues among them is the baryon asymmetry of the universe (BAU) [1, 2]:

$$Y_B \equiv \frac{\rho_B}{s} = \begin{cases} (8.2 - 9.4) \times 10^{-11} & (95\%CL), \text{ Big Bang Nucleosynthesis} \\ 8.65 \pm 0.09 \times 10^{-11}, & \text{PLANCK} \end{cases} \quad (1)$$

where ρ_B is the baryon number density, and s is the entropy density of the universe. The matter-antimatter asymmetry provided by the SM's CP-violating (CPV) is not of the required magnitude, this indicates the presence of new physics (NP) beyond the SM. Explaining baryon asymmetry by electroweak baryogenesis (EWBG) necessitates new CPV effects to theoretically amplify the EWBG responsible for generating the matter-antimatter asymmetry [3], which is also one of the most intriguing explanations for the origin of the asymmetry between matter and antimatter in cosmology.

The new CPV phases can not only provide many orders of magnitude higher matter-antimatter asymmetry than the SM predicts, but also yield larger values of the EDM than those predicted by the SM. In the SM, the predicted value of the electron EDM is approximately $10^{-38}e \cdot \text{cm}$ [4–6], yet it has not been detected by current experimental methods. However, when new CPV phases are introduced, the electron EDM can be enhanced by several orders of magnitude, and it is quite possible to be detected in the near future. Such observations would provide compelling evidence for the existence of NP beyond the SM. The upper bounds on the electron EDM d_e have been presented in Refs. [7, 8]

$$|d_e| < 4.1 \times 10^{-30}e \cdot \text{cm}. \quad (2)$$

In addition, the neutron EDM d_n and the mercury EDM d_{Hg} will also impose strict constraints on the parameter space of the new model, with the relevant experimental data provided by Ref. [7]

$$\begin{aligned} |d_{Hg}| &< 7.4 \times 10^{-30}e \cdot \text{cm}, \\ |d_n| &< 1.8 \times 10^{-26}e \cdot \text{cm}. \end{aligned} \quad (3)$$

It is evident that the experimental upper bounds on the electron EDM are quite stringent, thereby imposing tight constraints on any new sources of CPV. On the other hand, investigating the impact of NP effects on the electron EDM could contribute significantly to the understanding of the mechanisms underlying CPV.

Among the myriad extensions of the SM, supersymmetry stands out as one of the most popular candidates. The EWBG analysis within the MSSM has been thoroughly discussed in Refs. [9–21], while the EWBG analysis in non-minimal supersymmetric models has been elaborately addressed in Refs. [22–26]. In summary, the results indicate that the primary contributions to Y_B predominantly arise from the T-term (the trilinear scalar term in the soft supersymmetry-breaking potential) and the μ -term (the bilinear Higgs mass terms in the superpotential). The impact of supersymmetry effects on the electron EDM has been investigated in the referenced studies [27–41]. The results suggest that the cancellation of contributions from different phases is the most plausible explanation for suppressing the electron EDM below the corresponding experimental upper limits. Moreover, this cancellation is very stringent, generally reaching the level of 1%. When it is assumed that only the CPV phases originate from the T-term and the μ -term, their values are strictly constrained by the experimental upper bounds. Overall, studying the EWBG and the electron EDM in a combined way in NP models is of great interest, and will deepen our understanding of CPV.

The TNMSSM is an extension that amalgamates two expansions of the MSSM, namely the NMSSM and the TMSSM. This model alleviates the little hierarchy problem by introducing two scalar triplets and makes the μ term coincide with the soft SUSY breaking scale naturally by introducing a scalar singlet [42–51]. Correspondingly, new CPV sources are introduced in this model, and these TNMSSM specific CPV sources affect baryon asymmetry Y_B and the electron EDM d_e . Hence, we focus on explaining the impacts of CPV sources in the TNMSSM on Y_B and d_e in this work.

The organization of this paper is as follows. In Section 2, we provide a brief description of the TNMSSM by introducing the superpotential and the general soft-breaking terms. Then, in Section 3, we analyze the electroweak phase transition (EWPT), the Y_B , the electron EDM d_e , the neutron EDM d_n and mercury EDM d_{Hg} within the TNMSSM. In Section 4,

we explore the impact of CPV on the Y_B , electron EDM d_e , neutron EDM d_n and mercury EDM d_{Hg} by varying different parameters. The conclusions are summarized in Section 5.

II. THE TNMSSM

Like any general softly broken supersymmetric theory, the Lagrangian of the TNMSSM is characterized by the superpotential, supersymmetric gauge interactions, and various soft-breaking couplings (soft masses and trilinear terms). In the TNMSSM, a gauge singlet superfield S is introduced, along with two triplet superfields T and \bar{T} . The corresponding superpotential is given by Ref. [42]

$$W = S (\lambda H_u \cdot H_d + \lambda_T \text{tr}(\bar{T}T)) + \frac{\kappa}{3} S^3 + \chi_u H_u \cdot \bar{T} H_u + \chi_d H_d \cdot T H_d + Y_u H_u \cdot Q \bar{u} - Y_d H_d \cdot Q \bar{d} - Y_e H_d \cdot L \bar{e}, \quad (4)$$

where λ , λ_T , κ , χ_u , and χ_d are dimensionless Yukawa couplings. And the triplet superfields with hypercharge $Y = \pm 1$ are defined as follows:

$$T \equiv T^a \sigma^a = \begin{pmatrix} T^+/\sqrt{2} & -T^{++} \\ T^0 & -T^+/\sqrt{2} \end{pmatrix}, \quad (5)$$

$$\bar{T} \equiv \bar{T}^a \sigma^a = \begin{pmatrix} \bar{T}^-/\sqrt{2} & -\bar{T}^0 \\ \bar{T}^{--} & -\bar{T}^-/\sqrt{2} \end{pmatrix}, \quad (6)$$

where σ^a are the usual 2×2 Pauli matrices, and the respective definitions of the products between two $SU(2)_L$ doublets and between two $SU(2)_L$ doublets with one $SU(2)_L$ triplet are given as

$$H_u \cdot H_d = H_u^+ H_d^- - H_u^0 H_d^0, \quad (7)$$

$$H_u \cdot \bar{T} H_u = \sqrt{2} H_u^+ H_u^0 \bar{T}^- - (H_u^0)^2 \bar{T}^0 - (H_u^+)^2 \bar{T}^{--}, \quad (8)$$

$$H_d \cdot T H_d = \sqrt{2} H_d^- H_d^0 T^+ - (H_d^0)^2 T^0 - (H_d^-)^2 T^{++}. \quad (9)$$

The soft terms in the Lagrangian include:

$$\begin{aligned}
-\mathcal{L}_{\text{soft}} = & m_{H_u}^2 |H_u|^2 + m_{H_d}^2 |H_d|^2 + m_S^2 |S|^2 + m_T^2 \text{tr}(|T|^2) + m_{\bar{T}}^2 \text{tr}(|\bar{T}|^2) \\
& + m_Q^2 |Q|^2 + m_{\bar{u}}^2 |\bar{u}|^2 + m_{\bar{d}}^2 |\bar{d}|^2 + m_L^2 |L|^2 + m_{\bar{e}}^2 |\bar{e}|^2 \\
& + (T_u Q \cdot H_u \bar{u} - T_d Q \cdot H_d \bar{d} - T_e L \cdot H_d \bar{e} \\
& + A_S H_u \cdot H_d + A_T S \text{tr}(T\bar{T}) + \frac{A_\kappa}{3} S^3 + A_u H_u \cdot \bar{T} H_u + A_d H_d \cdot T H_d + h.c.). \tag{10}
\end{aligned}$$

The $SU(2)_L \otimes U(1)_Y$ electroweak symmetry breaking occurs when the neutral parts of Higgs fields obtain the VEVs

$$\begin{aligned}
H_d^0 &= \frac{1}{\sqrt{2}}(v_1 + \Re H_d^0 + i\Im H_d^0), & H_u^0 &= \frac{1}{\sqrt{2}}(v_2 + \Re H_u^0 + i\Im H_u^0), \\
T^0 &= \frac{1}{\sqrt{2}}(v_{T_1} + \Re T^0 + i\Im T^0), & \bar{T}^0 &= \frac{1}{\sqrt{2}}(v_{T_2} + \Re \bar{T}^0 + i\Im \bar{T}^0), \\
S &= \frac{1}{\sqrt{2}}(v_S + \Re S + i\Im S). \tag{11}
\end{aligned}$$

For convenience, we define $v_T^2 = v_{T_1}^2 + v_{T_2}^2$, $v^2 = v_1^2 + v_2^2$ and $\tan \beta' = \frac{v_{T_2}}{v_{T_1}}$ in analogy to the ratio of the MSSM VEVs ($\tan \beta = \frac{v_2}{v_1}$).

In the TNMSSM, the masses of the Z and W bosons are modified due to the presence of the triplet VEVs

$$M_Z^2 = \frac{g_1^2 + g_2^2}{4} u^2 \equiv \hat{g}^2 u^2, \tag{12}$$

$$M_W^2 = \frac{g_2^2}{4} (v_1^2 + v_2^2 + 2v_{T_1}^2 + 2v_{T_2}^2), \tag{13}$$

$$u^2 = v_1^2 + v_2^2 + 2v_{T_1}^2 + 2v_{T_2}^2 \approx (246 \text{ GeV})^2, \tag{14}$$

where g_1 and g_2 represent the gauge coupling constants of $U(1)_Y$ and $SU(2)_L$ respectively.

As mentioned in the introduction, the TNMSSM model addresses the μ problem(s) and the little hierarchy problem by incorporating additional singlet and triplet superfields. Regarding the μ problem(s), the vacuum expectation value v_s of the singlet field S will generate effective μ term for the Higgs doublet and triplet with

$$\mu = \lambda v_s, \quad \mu_T = \lambda_T v_s. \tag{15}$$

we take μ , v_s as inputs in the following analy analysis and λ is obtained by $\lambda = \frac{\mu}{v_s}$. For the little hierarchy problem, it can be clearly seen that the coupling of the triplet to the up -type

Higgs H_u introduces additional quartic couplings in the Higgs (tree-level) potential without mixing with the *down*-type Higgs H_d :

$$V_{\text{Higgs}} \ni \sim \chi_u^2 (H_u)^4. \quad (16)$$

The introduction of two triplets and a singlet, in addition to solving the μ problem and the little hierarchy problem, also enables some other interesting work, such as studies related to Higgs decay and the transition magnetic moments of Majorana neutrinos [52–55]. When scalar triplets are introduced, neutrinos can acquire Majorana masses through the type-II see-saw mechanism.

Compared to the MSSM, the TNMSSM superpotential introduces an additional physical CPV phase through the $Arg(\chi_u \chi_d \kappa \lambda_T^* (\lambda^*)^2)$. Notably, this will have an impact on the theoretical predictions for Y_B and electron EDM d_e within the TNMSSM.

III. EWBG AND ELECTRON EDM IN THE TNMSSM

In this section, we present the mechanism by which a strong first-order PT is achieved in the TNMSSM model, as well as the methodology for calculating the baryon asymmetry Y_B , the electron EDM d_e , the neutron EDM d_n and the mercury EDM d_{Hg} .

A. Electroweak phase transition

The EWPT is a pivotal process in the early universe's transition from a high-temperature symmetric phase to a low-temperature broken phase. This transition involves the development of the Higgs field vacuum expectation value, leading to the spontaneous breaking of electroweak symmetry. When the universe cooled below the electroweak scale temperature, broken phase bubbles began to nucleate in the symmetric plasma and rapidly expand. CP asymmetry was generated through interactions with the bubble walls, leading to a baryon number density asymmetry in the symmetric phase ahead of the bubble wall. These baryon number density asymmetries would diffuse into the region ahead of the bubble wall and affect electroweak sphaleron transitions, producing more baryons than antibaryons. Eventually, as the bubbles expanded and merged, the entire universe transitioned into the broken phase,

with the baryon number being preserved within the bubble walls due to the suppression of sphaleron transition rates. Successful EWBG requires a strong first-order EWPT, which typically necessitates new physics beyond the SM to achieve [56–59].

In the context of the MSSM, the discovery of the 125 GeV Higgs boson has rendered it improbable to have a strongly first-order EWPT with a very light right-handed stop of less than 120 GeV, thereby effectively ruling out the possibility of EWBG [60–69]. Compared to the MSSM, the TNMSSM, with the presence of the new singlet S , can realize a strong first-order phase transition. For simplicity, the temperature dependence of the Higgs VEVs β, β' is neglected and the tree-level effective potential can be represented as

$$V_{eff}(h, \eta, S) = M(T)^2 h^2 + m_\eta^2 \eta^2 + m_s^2 S^2 + \frac{1}{8}(g_1^2 + g_2^2)(h^2 \cos 2\beta + 2\eta^2 \cos 2\beta')^2 + \frac{2}{3} A_\kappa S^3, \quad (17)$$

where

$$\begin{aligned} M(T)^2 &\equiv M_0^2 + \mathcal{Q}T^2 \\ &= m_1^2 \cos^2 \beta + m_2 \sin^2 \beta + \lambda^2 S^2 + \kappa S^2 \lambda \sin 2\beta + \frac{1}{2} \lambda \sin 2\beta \lambda_T \eta^2 \sin^2 \beta' \\ &\quad + 2\lambda_T S \eta \sin \beta' \chi_d \sin \beta + 2\lambda_T S \eta \cos \beta' \chi_u \cos^2 \beta + 4\chi_u^2 \cos^2 \beta \eta^2 \sin^2 \beta' \\ &\quad + 2\lambda S \sin 2\beta \chi_u \eta \sin \beta' + 2\lambda S \sin 2\beta \chi_d \eta \cos \beta' - AS \sin 2\beta - 2A_u \cos^2 \beta \eta \sin \beta' \\ &\quad - 2A_d \sin^2 \beta \eta \cos \beta' + 4\chi_d^2 \sin^2 \beta \cos^2 \beta' + \mathcal{Q}T^2, \end{aligned} \quad (18)$$

$$\begin{aligned} m_\eta^2 &= \frac{1}{2} \lambda h^2 \sin 2\beta \lambda_T \sin^2 \beta' - \kappa S^2 \lambda_T \sin^2 \beta' + \lambda_T^2 S^2 + 4\chi_u^2 \cos^2 \beta \eta^2 \sin^2 \beta' \\ &\quad + S 4\chi_d^2 \sin^2 \beta \cos^2 \beta' - A_t S \sin 2\beta' + m_T \cos^2 \beta' + m_T^2 \sin^2 \beta', \end{aligned} \quad (19)$$

$$m_S^2 = \kappa \lambda h^2 \sin 2\beta - \kappa \lambda_T \sin^2 \beta' + \lambda_T \eta^2 + \lambda^2 h^2 + m_s^2, \quad (20)$$

and \mathcal{Q} represents the sum of relevant thermal coupling, T denotes temperature, h and η acquire VEVs $\langle h \rangle = v$, $\langle \eta \rangle = v_T$ respectively at zero temperature (present universe). At extremely high temperatures, h , η and S are stable at the origin. As the universe cooled, upon reaching the critical temperature for the phase transition, the Higgs field spontaneously broke the symmetry acquiring a non-zero vacuum expectation value, as shown in Fig. 1.

Furthermore, it can be noted in the Eqs. (17, 18) indicate that the only gauge-independent term possible is $\mathcal{Q}T^2$, and the gauge independence of the $\mathcal{O}(T^2)$ term has

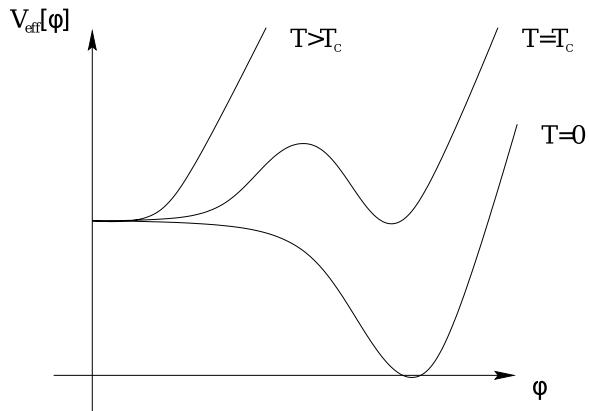


FIG. 1: First-order phase transition, the Higgs vacuum expectation value changes with the cooling of temperature as shown in the schematic diagram. The Higgs vacuum expectation value $v(T)$ at $T = T_C$ is defined as the temperature where the trivial and non-trivial minimum values are degenerate. From Ref. [59].

been demonstrated in Appendix C of Ref. [70]. Therefore, the EWPT in our analysis is gauge invariant. In the early formation of the universe, as the temperature decreased, the Higgs field expectation value abruptly jumped from zero to a non-zero value, achieving a strong first-order PT at temperature $T \sim m_W$. Subsequently, we can obtain T by solving the equations

$$\begin{cases} \left. \frac{\partial V_{eff}}{\partial h} \right|_{(v_c, v_{T_c})}^{T_c} = 0, \\ V_{eff}(h, \eta, S) = 0. \end{cases} \quad (21)$$

As stated at the beginning of this section, for EWBG to occur, the sphaleron process must decouple once the phase transition is complete. In other words, at that moment, the sphaleron rate in the broken phase should be smaller than the Hubble parameter. In general, the sphaleron decoupling condition is cast into the form $v(T_C)/T_C \gtrsim 1$. And in the parameter space selected in the following section of our analysis, we have $v(T_C)/T_C \gtrsim 1.3$. This is sufficient for EWBG to occur.

B. Baryon asymmetry Y_B

Investigating the relationship between CPV effects and quantum transport equations is a complex and important aspect of research into EWBG. CPV effects act as source terms in the quantum transport equations that govern the generation of chiral charge at phase boundaries. In the TNMSSM model, the natural encoding of many CPV phases, such as κ , χ_d , χ_d , μ , T_u , T_d , T_e , is considered. Among these, the phase μ , T_u , T_d , T_e have significant impact on the generation of Y_B . According to Ref. [13], the expression for the baryon-to-entropy ratio can be simplified to

$$Y_B = F_1 \sin \theta_\mu + F_2 \sin(\theta_\mu + \theta_T). \quad (22)$$

where we have taken the gaugino mass terms $M_{1,2}$ to be real. And the phases μ and T are two independent CPV phases that influence baryon asymmetry and electron EDM d_e within the model. The coefficients F_i depend on the mass parameters in the TNMSSM, such as μ , M_1 , M_2 , T_0 (we assume that T-terms are all same at the GUT scale, $T_u/Y_u = T_d/Y_d = T_e/Y_e = T_0$, where $Y_{u,d,e}$ are the corresponding Yukawa coupling constants) and squark masses $M_{\tilde{t}_L}$, $M_{\tilde{t}_R}$ [71]. Furthermore, F_i also have a overall dependence on bubble wall parameters v_w , L_w , $\Delta\beta$. For Eq. (22), the detailed parameters used, such as the bubble wall parameter v_w , L_w and $\Delta\beta$ are calculated with Ref. [72], the thermal width with Ref. [73, 74], and the diffusion constant is selected with Refs. [75, 76]. The relevant thermal parameters we have chosen will also be provided in Appendix A.

C. The EDM of electron d_e , d_n and d_{Hg}

The effective Lagrangian for the electron EDM can be written as

$$\mathcal{L}_{EDM} = -\frac{i}{2} d_e \bar{l}_e \sigma^{\mu\nu} \gamma_5 l_e F_{\mu\nu}, \quad (23)$$

where $\sigma^{\mu\nu} = i[\gamma^\mu, \gamma^\nu]/2$, $F_{\mu\nu}$ is the electromagnetic field strength, and l_e denotes the electron which is on-shell.

When the internal mass m_v is much larger than the external electron mass m_e , the effective Lagrangian method can conveniently be used to obtain the contribution of loop

diagrams to the EDM. Since $\not{p} = m_e \ll m_\nu$ for on-shell electron and $\not{k} \rightarrow 0 \ll m_\nu$ for photon, we can expand the amplitude of corresponding Feynman diagrams according to the external momenta of electron and photon. After matching the effective theory with the full theory, one obtains the high-dimensional operators and their coefficients. In subsequent calculations, it is sufficient to retain only these 6-dimensional operators [77–80]:

$$\begin{aligned}
O_2^{L,R} &= \frac{eQ_f}{(4\pi)^2} \overline{(i\mathcal{D}_\mu l_e)} \gamma^\mu F \cdot \sigma P_{L,R} l_e, \\
O_3^{L,R} &= \frac{eQ_f}{(4\pi)^2} \bar{l}_e F \cdot \sigma \gamma^\mu P_{L,R} (i\mathcal{D}_\mu l_e), \\
O_6^{L,R} &= \frac{eQ_f m_e}{(4\pi)^2} \bar{l}_e F \cdot \sigma P_{L,R} l_e,
\end{aligned} \tag{24}$$

where $\mathcal{D}_\mu = \partial^\mu + ieA_\mu$, $P_L = \frac{1}{2}(1 - \gamma_5)$, $P_R = \frac{1}{2}(1 + \gamma_5)$, e represents the electric charge, $Q_f = -1$ represents the charge number of electron and m_e is the mass of electron l_e . The 6-dimensional operator in Eq. (24) induce the effective coupling between the photon and the electron. The effective vertex with one external photon can be written as

$$\begin{aligned}
O_2^{L,R} &= \frac{ieQ_f}{(4\pi)^2} (\not{p} + \not{k}) [\not{k}, \gamma_\rho] P_{L,R}, \\
O_3^{L,R} &= \frac{ieQ_f}{(4\pi)^2} [\not{k}, \gamma_\rho] \not{p} P_{L,R}, \\
O_6^{L,R} &= \frac{ieQ_f m_e}{(4\pi)^2} [\not{k}, \gamma_\rho] P_{L,R}.
\end{aligned} \tag{25}$$

If the full theory is invariant under the combined transformation of charge conjugation, parity and time reversal (CPT), the induced effective theory preserves the symmetry after the heavy freedoms are integrated out. The fact implies the Wilson coefficients of the operators $O_{2,3,6}^{L,R}$ satisfying the relations [77, 80]

$$C_3^{L,R} = C_2^{R,L*}, \quad C_6^L = C_6^{R*}, \tag{26}$$

where $C_i^{L,R}$ represent the Wilson coefficients of the corresponding operators $O_i^{L,R}$ in the effective Lagrangian. After applying the equations of motion to the external electron, we

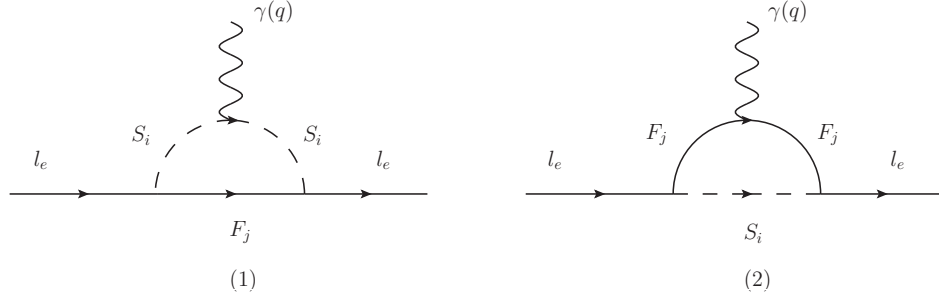


FIG. 2: The one-loop Feynman diagrams contributing to the electron EDM, where (1) denotes a charged scalar loop, and (2) denotes a charged fermion loop.

find that the concerned terms in the effective Lagrangian are transformed into

$$\begin{aligned}
& C_2^L O_2^L + C_2^{R*} O_3^L + C_6^{R*} O_6^L \\
& \Rightarrow (C_2^{R*} + C_2^L + C_6^{R*}) O_6^L \\
& = \frac{ieQ_f m_e}{(4\pi)^2} \Im(C_2^R + C_2^{L*} + C_6^R) \bar{l}_e \sigma^{\mu\nu} \gamma_5 l_e F_{\mu\nu},
\end{aligned} \tag{27}$$

where, $\Im(\dots)$ denotes the operation to take the imaginary part of a complex number. Matching between Eq. (23) and Eq. (27), we can obtain

$$d_e = -\frac{2eQ_f m_e}{(4\pi)^2} \Im(C_2^R + C_2^{L*} + C_6^R), \tag{28}$$

Next we will analyse the dominant one-loop diagrams contributing to the electron EDM d_e in the TNMSSM, which are depicted by Fig. 2. Calculating the Feynman diagrams, the electron EDM d_e can be written as

$$\begin{aligned}
d_e^{(1)} = & \frac{-2}{em_e} \Im \left\{ x_e [-I_3(x_{F_j}, x_{S_i}) + I_4(x_{F_j}, x_{S_i})] [(C_{\bar{l}_e S_i F_j}^L C_{\bar{F}_j S_i l_e}^R) + (C_{\bar{l}_e S_i F_j}^R C_{\bar{F}_j S_i l_e}^L)^*] \right. \\
& \left. + \sqrt{x_e x_{F_j}} [-2I_1(x_{F_j}, x_{S_i}) + 2I_3(x_{F_j}, x_{S_i})] C_{\bar{l}_e S_i F_j}^R C_{\bar{F}_j S_i l_e}^R \right\},
\end{aligned} \tag{29}$$

$$\begin{aligned}
d_e^{(2)} = & \frac{-2}{em_e} \Im \left\{ x_e [-I_1(x_{F_j}, x_{S_i}) + 2I_3(x_{F_j}, x_{S_i}) - I_4(x_{F_j}, x_{S_i})] [(C_{\bar{l}_e S_i F_j}^R C_{\bar{F}_j S_i l_e}^L) \right. \\
& \left. + (C_{\bar{l}_e S_i F_j}^L C_{\bar{F}_j S_i l_e}^R)^*] + \sqrt{x_e x_{F_j}} [2I_1(x_{F_j}, x_{S_i}) - 2I_2(x_{F_j}, x_{S_i}) - 2I_3(x_{F_j}, x_{S_i})] \right. \\
& \left. \times C_{\bar{l}_e S_i F_j}^R C_{\bar{F}_j S_i l_e}^R \right\},
\end{aligned} \tag{30}$$

where $x_i = m_i^2/m_W^2$, $C_{abc}^{L,R}$ denotes the constant parts of the interactional vertex about abc , which can be got through SARAH, the interacting particles are denoted by a, b, c . And the

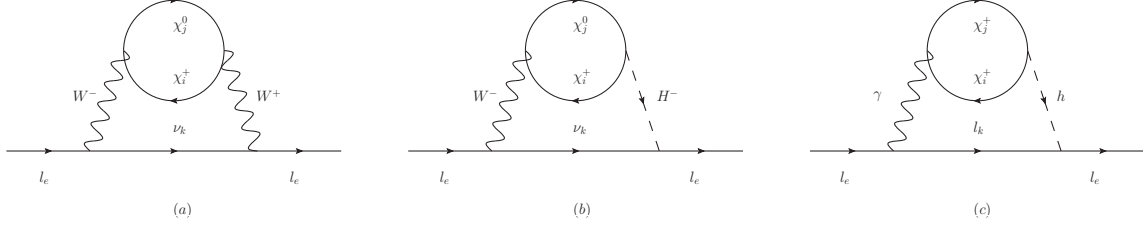


FIG. 3: The two-loop Barr-Zee diagrams, where one closed fermion loop is connected to virtual gauge bosons or the Higgs field, provide corresponding contributions to d_e by attaching photons to the internal particles in all possible ways.

specific expressions for the functions $I_{1,2,3}(x_1, x_2)$ is given by Refs. [81, 82]. For completeness, we will provide the specific forms of $C_{abc}^{L,R}$ and $I_{1,2,3}(x_1, x_2)$ in Appendix B.

The two-loop Barr-Zee diagrams can provide corrections to the electron EDM d_e . Here, we consider the contributions from two-loop diagrams where closed fermion loops are connected to virtual gauge bosons or the Higgs field. According to Ref. [83], the Feynman diagrams are shown in Fig. 3. Assuming $m_F = m_{\chi_i^+} = m_{\chi_j^0} \gg m_W$, $m_F = m_{\chi_i^+} \gg m_h$, the contributions from the two-loop diagrams to d_e can be simplify as

$$\begin{aligned}
d_e^{(a)} &= \frac{3G_F m_W \sqrt{x_e}}{-64\sqrt{2}\pi^4} \left\{ \Im(C_{f_j W f_i}^L C_{f_j W f_i}^{R*}) \right\}, \\
d_e^{(b)} &= \frac{G_F e m_W C_{l_e H \nu_k}^L}{256\pi^4 g_2 \sqrt{x_F}} \left\{ \left[179/36 + 10/3 J(x_F, x_W, x_H) \right] \Im(C_{f_i H f_j}^L C_{f_j W f_i}^L + C_{f_i H f_j}^R C_{f_j W \chi_i^+}^R) \right. \\
&\quad + \left[-1/9 - 2/3 J(x_F, x_W, x_H) \right] \Im(C_{f_i H f_j}^L C_{f_j W f_i}^R + C_{f_i H f_j}^R C_{f_j W f_i}^L) \\
&\quad + \left[-16/9 - 8/3 J(x_F, x_W, x_H) \right] \Im(C_{f_i H f_j}^L C_{f_j W f_i}^L - C_{f_i H f_j}^R C_{f_j W \chi_i^+}^R) \\
&\quad \left. + \left[-2/9 - 4/3 J(x_F, x_W, x_H) \right] \Im(C_{f_i H f_j}^L C_{f_j W f_i}^R - C_{f_i H f_j}^R C_{f_j W f_i}^L) \right\}, \\
d_e^{(c)} &= \frac{G_F e m_W C_{l_e h^0 l_e}^L}{64\pi^4 \sqrt{x_F}} \Im(C_{f_i h^0 f_i}^L) \left[1 + \ln \frac{x_F}{x_h} \right], \tag{31}
\end{aligned}$$

where f_j, f_i denote χ_j^0 and χ_i^\pm respectively, W denotes W boson, H denotes charged Higgs boson, h denotes SM-like Higgs boson, the concrete expressions for the function J can be found in Ref. [84], and we will also provide it in the Appendix B.

In addition to the constraints from the electron EDM d_e on the new model, the neutron EDM d_n and the mercury EDM d_{Hg} also impose strict limits on the parameter space. We briefly discuss the neutron EDM d_n and the mercury EDM d_{Hg} here.

The EDM of neutron d_n can be expressed in terms of fundamental dipoles [85]

$$d_n = (1 \pm 0.5)[1.4(d_d^\gamma - 0.25d_u^\gamma) + 1.1e(d_d^g + 0.5d_u^g)] \pm (22 \pm 10) \text{ MeV}C_5, \quad (32)$$

where d_q^γ , d_q^g , C_5 denote the quark EDM of q from the electroweak interaction, the CEDM of q and the coefficient of Weinberg operator at the chirality scale respectively. Using the running from Refs. [86, 87] at one-loop, $d_{d,u}^{\gamma,g}$ and C_5 can be expressed in terms of d_c^g at the scale m_c [88]. The values of the coefficients 1 ± 0.5 and 22 ± 10 MeV are respectively adopted as 0.5 and 12 MeV.

The effective Lagrangian for the quark EDMs can be written as

$$\mathcal{L}_{EDM} = -\frac{i}{2}d_q^\gamma \bar{q} \sigma^{\mu\nu} \gamma_5 q F_{\mu\nu}, \quad (33)$$

where $\sigma^{\mu\nu} = i[\gamma^\mu, \gamma^\nu]/2$, q is the wave function for quark, and $F_{\mu\nu}$ is the electromagnetic field strength. Adopting the effective Lagrangian approach, the quark EDMs can be written as

$$d_q^\gamma = -\frac{2eQ_q m_q}{(4\pi)^2} \Im(C_2^R + C_2^{L*} + C_6^R), \quad (34)$$

where $C_{2,6}^{L,R}$ represent the Wilson coefficients of the corresponding operators $O_{2,6}^{L,R}$

$$\begin{aligned} O_2^{L,R} &= \frac{eQ_q}{(4\pi)^2} (-iD_\alpha^*) \bar{q} \gamma^\alpha F \cdot \sigma P_{L,R} q, \\ O_6^{L,R} &= \frac{eQ_q m_q}{(4\pi)^2} \bar{q} F \cdot \sigma P_{L,R} q. \end{aligned} \quad (35)$$

Similarly, the effective Lagrangian for the quark CEDMs can be written as

$$\mathcal{L}_{CEDM} = -\frac{i}{2}d_q^g \bar{q} \sigma^{\mu\nu} \gamma_5 q G_{\mu\nu}^a T^a, \quad (36)$$

where $G_{\mu\nu}$ is the $SU(3)$ gauge field strength, T^a is the $SU(3)$ generators. Then the quark CEDMs can be written as

$$d_q^g = -\frac{2g_3 m_q}{(4\pi)^2} \Im(C_7^R + C_7^{L*} + C_8^R), \quad (37)$$

where $C_{7,8}^{L,R}$ represent the Wilson coefficients of the corresponding operators $O_{7,8}^{L,R}$

$$\begin{aligned} O_7^{L,R} &= \frac{g_3}{(4\pi)^2} (-iD_\alpha^*) \bar{q} \gamma^\alpha G^a \cdot \sigma T^a P_{L,R} q, \\ O_8^{L,R} &= \frac{g_3 m_q}{(4\pi)^2} \bar{q} G^a \cdot \sigma T^a P_{L,R} q. \end{aligned} \quad (38)$$

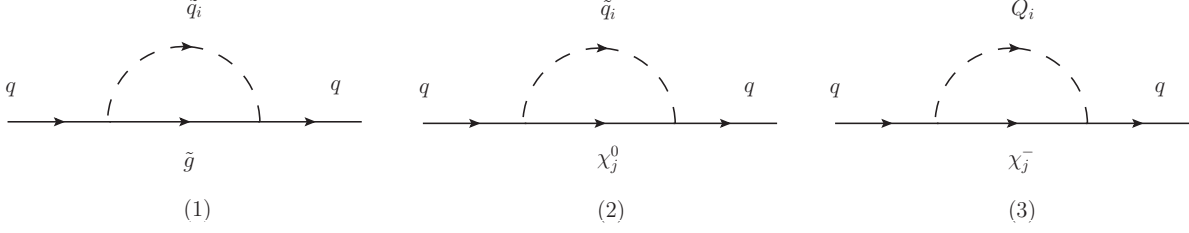


FIG. 4: The one-loop diagrams which contributes to d_q^γ and d_q^g are obtained by attaching a photon and a gluon respectively to the internal particles in all possible ways.

The one-loop Feynman diagrams contributing to the above amplitude are shown in Fig. 4. When calculating the Feynman diagrams, d_q^γ and d_q^g at the one-loop level can be written as

$$\begin{aligned}
d_q^{\gamma(1)} &= \frac{e_q e}{12\pi^2 m_W} \frac{\sqrt{x_{\tilde{g}}}}{x_{\tilde{q}_i}} \Im \left[C_{\tilde{g}\tilde{q}_i q}^L C_{\tilde{q}\tilde{q}_i \tilde{g}}^L \right] I_1 \left(\frac{x_{\tilde{g}}}{x_{\tilde{q}_i}} \right), \\
d_q^{g(1)} &= \frac{-g_3}{32\pi^2 m_W} \frac{\sqrt{x_{\tilde{g}}}}{x_{\tilde{q}_i}} \Im \left[C_{\tilde{g}\tilde{q}_i q}^L C_{\tilde{q}\tilde{q}_i \tilde{g}}^L \right] I_2 \left(\frac{x_{\tilde{g}}}{x_{\tilde{q}_i}} \right), \\
d_q^{\gamma(2)} &= \frac{e_q e}{32\pi^2 m_W} \frac{\sqrt{x_{\chi_j^0}}}{x_{\tilde{q}_i}} \Im \left[C_{\tilde{q}\tilde{q}_i \chi_j^0}^L C_{\tilde{\chi}_j^0 \tilde{q}_i q}^R \right] I_1 \left(\frac{x_{\chi_j^0}}{x_{\tilde{q}_i}} \right), \\
d_q^{g(2)} &= \frac{g_3^3}{128\pi^2 e^2 m_W} \frac{\sqrt{x_{\chi_j^0}}}{x_{\tilde{q}_i}} \Im \left[C_{\tilde{q}\tilde{q}_i \chi_j^0}^L C_{\tilde{\chi}_j^0 \tilde{q}_i q}^R \right] I_1 \left(\frac{x_{\chi_j^0}}{x_{\tilde{q}_i}} \right), \\
d_q^{\gamma(3)} &= \frac{e}{16\pi^2 m_W} \frac{\sqrt{x_{\chi_j^-}}}{x_{\tilde{Q}_i}} \Im \left[C_{\tilde{q}\tilde{Q}_i \chi_j^-}^L C_{\tilde{\chi}_j^- \tilde{Q}_i q}^R \right] \left[e_Q I_1 \left(\frac{x_{\chi_j^-}}{x_{\tilde{Q}_i}} \right) + (e_q - e_Q) I_3 \left(\frac{x_{\chi_j^-}}{x_{\tilde{q}_i}} \right) \right], \\
d_q^{g(3)} &= \frac{g_3^3}{16\pi^2 e^2 m_W} \frac{\sqrt{x_{\chi_j^-}}}{x_{\tilde{Q}_i}} \Im \left[C_{\tilde{q}\tilde{Q}_i \chi_j^-}^L C_{\tilde{\chi}_j^- \tilde{Q}_i q}^R \right] I_1 \left(\frac{x_{\chi_j^-}}{x_{\tilde{Q}_i}} \right), \tag{39}
\end{aligned}$$

where x_i denotes m_i^2/m_W^2 , g_3 is the strong coupling constant, $C_{abc}^{L,R}$ denotes the constant parts of the interaction vertex about abc which can be obtained through SARAH, and a, b, c denote the interacting particles. We will provide the specific forms of $C_{abc}^{L,R}$ and $I_{1,2,3}(x)$ in Appendix B.

The two-loop gluon corrections to the Wilson coefficients in the quark self-energy diagrams are considered, and the corresponding Feynman diagrams are shown in Fig. 5. By attaching photons or gluons to internal particles in all possible ways, the corresponding dipole moment diagrams can be obtained. The contributions of the two-loop diagrams to

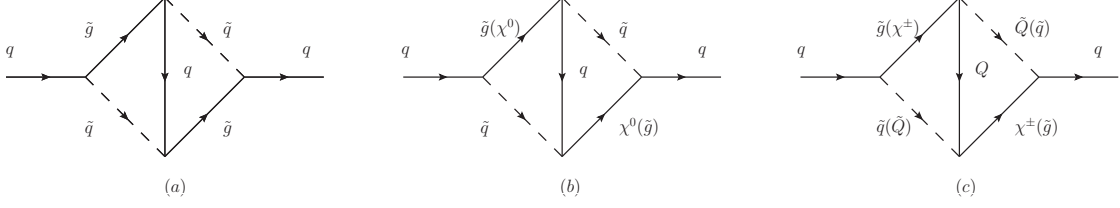


FIG. 5: The two-loop diagrams which contributes to d_q^γ and d_q^g are obtained by attaching a photon and a gluon respectively to the internal particles in all possible ways.

d_q^γ and d_q^g can be written as

$$\begin{aligned}
d_q^{\gamma(a)} &= \frac{-4e_q e g_3^2 |m_{\tilde{g}}|}{9(4\pi)^4 m_W^2} F_3(x_q, x_{\tilde{q}_j}, x_{\tilde{g}}, x_{\tilde{g}}, x_{\tilde{q}_i}) \Im[C_{\tilde{q}\tilde{g}\tilde{q}_j}^L C_{\tilde{g}\tilde{q}\tilde{q}_j}^L], \\
d_q^{g(a)} &= d_q^{\gamma(a)} g_3 / (e_q e), \\
d_q^{\gamma(b)} &= \frac{4e_q e}{3(4\pi)^4 m_W^2} \left\{ |m_{\tilde{g}}| F_4(x_q, x_{\tilde{q}_j}, x_{\tilde{g}}, x_{\chi_k^0}, x_{\tilde{q}_i}) \Im[C_{\tilde{\chi}_k^0 q \tilde{q}_j}^R C_{\tilde{\chi}_k^0 q \tilde{q}_i}^L C_{\tilde{g}\tilde{q}\tilde{q}_j}^L C_{\tilde{g}\tilde{q}\tilde{q}_i}^L - C_{\tilde{\chi}_k^0 q \tilde{q}_j}^L \right. \\
&\quad \times C_{\tilde{\chi}_k^0 q \tilde{q}_i}^R C_{\tilde{q}\tilde{g}\tilde{q}_j}^{L*} C_{\tilde{q}\tilde{g}\tilde{q}_i}^{L*}] - m_{\chi_k^0} F_5(x_q, x_{\tilde{q}_j}, x_{\tilde{g}}, x_{\chi_k^0}, x_{\tilde{q}_i}) \Im[C_{\tilde{\chi}_k^0 q \tilde{q}_j}^R C_{\tilde{\chi}_k^0 q \tilde{q}_i}^R C_{\tilde{q}\tilde{g}\tilde{q}_j}^{L*} C_{\tilde{q}\tilde{g}\tilde{q}_i}^L \\
&\quad \left. - C_{\tilde{\chi}_k^0 q \tilde{q}_j}^L C_{\tilde{\chi}_k^0 q \tilde{q}_i}^L C_{\tilde{q}\tilde{g}\tilde{q}_j}^{L*} C_{\tilde{q}\tilde{g}\tilde{q}_i}^L] \right\}, \\
d_q^{g(b)} &= d_q^{\gamma(b)} g_3 / (e_q e), \\
d_q^{\gamma(c)} &= \frac{2e}{3(4\pi)^4 m_W^2} \left\{ |m_{\tilde{g}}| F_4(x_Q, x_{\tilde{Q}_j}, x_{\tilde{g}}, x_{\chi_k^\pm}, x_{\tilde{q}_i}) \Im[C_{\tilde{Q}\tilde{\chi}_k^\pm \tilde{q}_j}^L C_{\tilde{Q}\tilde{\chi}_k^\pm \tilde{q}_i}^R C_{\tilde{g}\tilde{Q}\tilde{Q}_j}^L C_{\tilde{g}\tilde{Q}\tilde{Q}_i}^L - C_{\tilde{Q}\tilde{\chi}_k^\pm \tilde{q}_j}^R \right. \\
&\quad \times C_{\tilde{Q}\tilde{\chi}_k^\pm \tilde{q}_i}^L C_{\tilde{Q}\tilde{g}\tilde{Q}_j}^{L*} C_{\tilde{Q}\tilde{g}\tilde{Q}_i}^{L*}] - m_{\chi_k^\pm} F_5(x_Q, x_{\tilde{Q}_j}, x_{\tilde{g}}, x_{\chi_k^\pm}, x_{\tilde{q}_i}) \Im[C_{\tilde{Q}\tilde{\chi}_k^\pm \tilde{q}_j}^L C_{\tilde{Q}\tilde{\chi}_k^\pm \tilde{q}_i}^L C_{\tilde{Q}\tilde{g}\tilde{Q}_j}^{L*} C_{\tilde{Q}\tilde{g}\tilde{Q}_i}^L \\
&\quad \left. - C_{\tilde{Q}\tilde{\chi}_k^\pm \tilde{q}_j}^R C_{\tilde{Q}\tilde{\chi}_k^\pm \tilde{q}_i}^R C_{\tilde{g}\tilde{Q}\tilde{Q}_j}^L C_{\tilde{Q}\tilde{g}\tilde{Q}_i}^{L*}] \right\}, \\
d_q^{g(c)} &= d_q^{\gamma(c)} g_3 / e, \tag{40}
\end{aligned}$$

where the concrete expressions for the functions $F_{3,4,5}$ can be found in Ref. [89]. The similar expressions of two-loop gluino contributions can be found in Ref. [89]. We write these symbols in a general form to facilitate the calculation of the quark EDM in other NP models.

When SM quarks act as internal particles, there is an infrared divergence in Fig. 5, because we calculate these diagrams by extending the external momenta. In this case, it is necessary to match the complete theory diagrams with the corresponding two-loop diagrams in Fig. 5 to eliminate the infrared divergence. Taking Fig. 5(a) as an example, the method for eliminating infrared divergences is illustrated, with the corresponding schematic diagrams

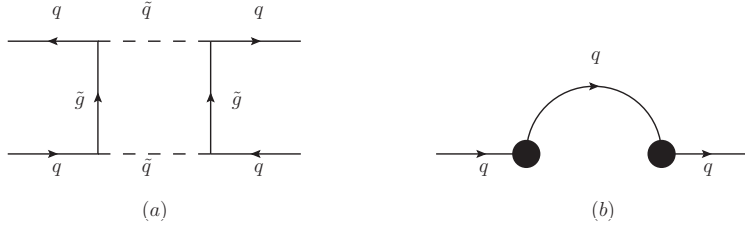


FIG. 6: Full theory diagram (a) and effective diagram (b) are plotted, where the blobs denote the effective vertexes, and a outgoing photon or gluon is attached by all possible ways.

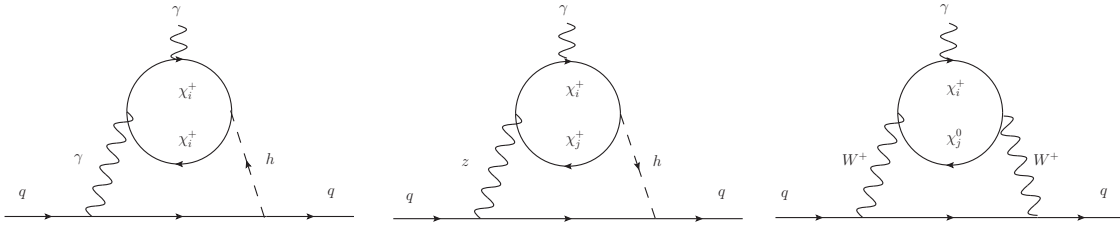


FIG. 7: The two-loop Barr-Zee type diagrams that contribute to the quark EDM. Diagrams where photons or gluons are emitted from the W boson or the internal fermion do not contribute to the quark EDM or CEDM.

shown in Fig. 6. When an external gluon is attached to the internal particles in Fig. 5(a), the external gluon can be attached to the same internal particles in Fig. 6(a) or (b). Then, the infrared divergence in the diagram of Fig. 5(a) with the attached gluon can be canceled by subtracting the corresponding diagrams in Fig. 6 with the gluon attached in the same manner.

The two-loop Barr-Zee-type diagrams can also provide corrections to the quark EDM. Consider the diagrams where a closed fermion loop is connected to a virtual gauge boson or Higgs field, as shown in Fig. 7. Then, the contribution of the two-loop Barr-Zee type

diagrams to is given by [90]

$$\begin{aligned}
d_q^{\gamma h} &= \frac{e_q e^3}{32\pi^4 m_W} \frac{\sqrt{x_{\chi_i^+}}}{x_{h_k}} \Im \left[C_{\bar{\chi}_i^+ h \chi_i^+}^R C_{\bar{q} h_k q} \right] f_{\gamma H} \left(\frac{x_{\chi_i^+}}{x_{h_k}} \right), \\
d_q^{Zh} &= \frac{e^2 (T_{3q} - 2e_q s_w^2)}{128\pi^4 c_w s_w m_W} \frac{\sqrt{x_{\chi_i^+}}}{x_{h_k}} \Im \left[\left(C_{\bar{\chi}_j^+ h_k \chi_i^+}^R C_{\bar{\chi}_i^+ Z \chi_j^+}^L - C_{\bar{\chi}_j^+ h_k \chi_i^+}^L C_{\bar{\chi}_i^+ Z \chi_j^+}^R \right) C_{\bar{q} h_k q} \right] \\
&\quad * f_{ZH} \left(\frac{x_Z}{x_{h_k}}, \frac{x_{\chi_i^+}}{x_{h_k}}, \frac{x_{\chi_j^+}}{x_{h_k}} \right), \\
d_q^{WW} &= \frac{T_{3q} e^3}{128\pi^4 s_w^2 m_W} \sqrt{x_q x_{\chi_i^+} x_{\chi_j^0}} \Im \left[C_{\bar{\chi}_j^0 W_\mu^+ \chi_i^+}^R C_{\bar{\chi}_j^0 W_\mu^+ \chi_i^+}^{L*} \right] f_{WW} \left(x_{\chi_i^+}, x_{\chi_j^0} \right), \tag{41}
\end{aligned}$$

where $s_w \equiv \sin \theta_W$, $c_w \equiv \cos \theta_W$, and θ_W is the Weinberg angle, T_{3q} denotes the isospin of the corresponding quark, the functions $f_{\gamma H}$, f_{ZH} , f_{WW} can be found in Ref. [90].

The EDM of mercury d_{Hg} is primarily contributed by the CEDM of quarks (d_q^g), which can be written as [13]

$$d_{Hg} = - (d_d^g - d_u^g - 0.012 d_s^g) \times 3.2 \cdot 10^{-2} e. \tag{42}$$

d_q^g can be obtained in Eq.(39), Eq.(40) and Eq.(41).

IV. NUMERICAL ANALYSES

In this section, we present and analyze the numerical results for the baryon asymmetry Y_B and the electron EDM d_e in the TNMSSM. The appropriate SM input parameters are selected as $m_W = 80.3692$ GeV, $m_Z = 91.1880$ GeV, $\alpha_{em}(m_Z) = 1/137$, $\alpha_s(m_Z) = 0.118$, we take the stop mass $m_{\tilde{t}_L} = m_{\tilde{t}_R} = 1.5$ TeV, charged Higgs boson mass $M_{H^\pm} = 1.5$ TeV for simplicity. According to Refs. [91–93], the magnitude of the scalar trilinear coupling is constrained by avoiding charge and color breaking minima. Thus, we take $T_0 = 0.1$ TeV to satisfy these conditions. The mass of the SM-like Higgs boson is 125 ± 0.2 GeV [7], which imposes stringent constraints on the parameter space. Compared to the MSSM, the new triplet and singlet particles mix with the MSSM scalar doublets at the tree level in the TNMSSM, thereby affecting the theoretical predictions for the mass of the SM-like Higgs boson. And within our chosen parameter space, the lightest Higgs mass in the TNMSSM is constrained in the range $124 \text{ GeV} < m_h < 126 \text{ GeV}$. Within our parameter space, we choose

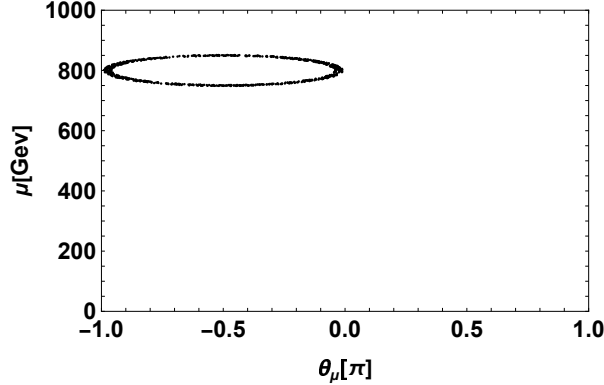


FIG. 8: Keeping Y_B in the region $(8.2 - 9.4) \times 10^{-11}$, the allowed region of θ_μ and μ .

$\tan \beta = 2$, $\tan \beta' = 0.8$, $M_{\tilde{L}, \tilde{e}} = \text{diag}(2, 2, 2)$ TeV. Taking into account the experimental constraints [7], we appropriately fix $M_1 = 600$ GeV and $M_2 = 800$ GeV for simplicity.

Considering the tree-level masses of W boson and Z boson, in the TNMSSM, the parameter ρ can be written as [94]

$$\rho = \frac{m_W^2}{\cos^2 \theta_W m_Z^2} = 1 - \frac{2v_T^2}{v^2}, \quad (43)$$

where θ_W is the Weinberg angle. The constraint on this parameter within 2σ -deviation requires $\rho_{\text{exp}} = 1.00038 \pm 0.00020 \times 2$ experimentally. Therefore, the scenario in which the value of v_T^2 does not exceed 1 GeV is safer.

In order to see how θ_μ , θ_{T_0} and μ affect Y_B , we scan the regions of the parameter space [$\theta_\mu = (-\pi, \pi)$, $\theta_{T_0} = (-\pi, \pi)$, $\mu = (100, 1000)$ GeV]. During the scanning process, we keep Y_B within the range of $(8.2 - 9.4) \times 10^{-11}$. The allowed regions for θ_μ and μ are shown in Fig. 8. From the figure, it is evident that an ellipse is formed in the negative θ_μ phase space near $\mu = 800$ GeV. According to the Refs. [13, 72, 95], a resonance behavior is induced when μ is approximately equal to M_2 , which can lead to an enhancement of the Y_B value. This is the reason why the ellipse is concentrated near $\mu = 800$ GeV. The concentration in the negative phase space arises because, in our Eq.(22), the F_1 term contributed by the S_H^{CP} source is negative, while Y_B is positive. This necessitates that the product $F_1 \sin \theta_\mu$ be positive, which naturally leads to the phase angle θ_μ being confined to the negative phase space. Through the memory effect, the required phase angle θ_μ can be reduced by two orders

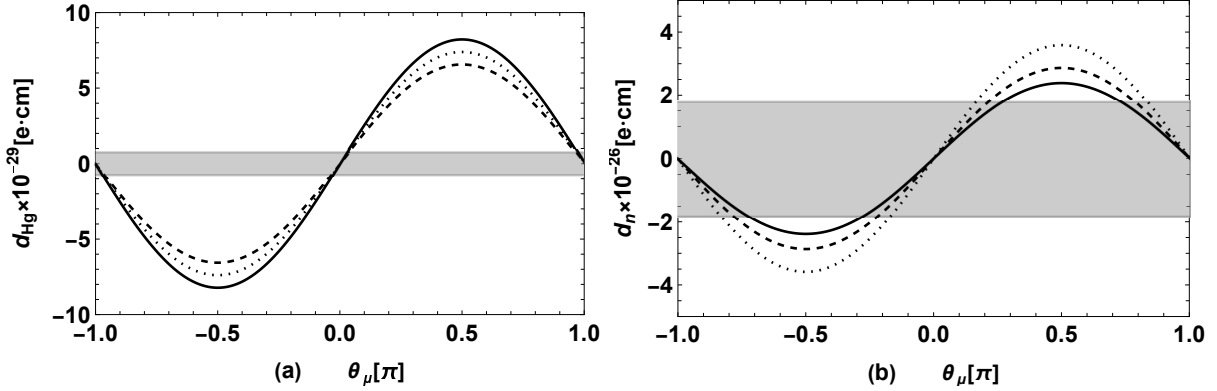


FIG. 9: (a) and (b) correspond to the results of the d_{Hg} and d_n scans in the parameter space, respectively. The solid line, dashed line, and dotted line correspond to $\mu = 800$ GeV, 900 GeV, 1000 GeV, respectively. The gray bands represent the experimental upper limits.

of magnitude. An elaborate explanation of this memory effect is detailed in Ref. [72], and the expression for determining whether it can occur can be succinctly expressed as

$$|\sin \theta_\mu| \gtrsim 10^{-3} \left(\frac{v_w}{0.1} \right). \quad (44)$$

it represents that the observed baryon asymmetry may be caused by Higgsinos. This reasonably explains why a small phase can successfully generate Y_B .

To better explain the EWBG, we have scanned the neutron EDM d_n and the mercury EDM d_{Hg} in the parameter space. The results are shown in the Fig. 9. This indicates that after considering the neutron EDM d_n and the mercury EDM d_{Hg} , the phase space of parameter μ will be further compressed.

Then we select $\mu = 800$ GeV and $|\theta_\mu| = 0.013$ to observe the effect of phase angle θ_{T_0} and new triplet couplings λ_T on Y_B . Y_B versus θ_{A_0} for $\lambda_T = 0.2$ (solid line), 0.3 (dashed line), 0.4 (dotted line) is plotted in Fig. 10, where the gray area denotes the experimental interval $(8.2 - 9.4) \times 10^{-11}$. From the experimental results, the sensitivity of Y_B to θ_{A_0} is less than its sensitivity to the new triplet coupling parameter λ_T . This indicates that while the contribution of the S_t^{CP} source to Y_B is not as significant as that of the S_H^{CP} source, it still exerts a certain influence on the outcome.

To better illustrate the stringent constraints on the new CP source contributions within

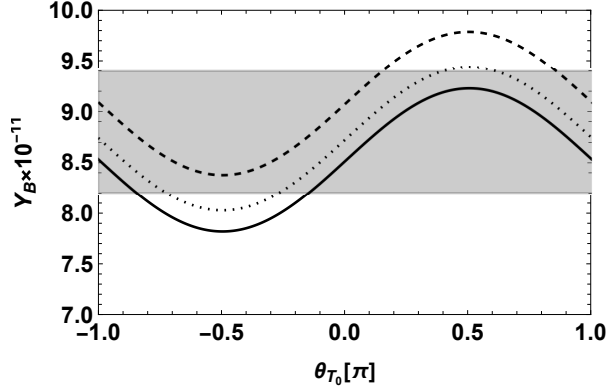


FIG. 10: Y_B versus θ_{T_0} for $\lambda_T = 0.2$ (solid line), 0.3 (dashed line), 0.4 (dotted line), and the gray area denotes the experimental interval $(8.2 - 9.4) \times 10^{-11}$.

the model, we have conducted a discussion on the electron EDM d_e , similar to that in Refs. [13, 71]. The numerical results for the Y_B indicate that when EWBG occurs, we chose $|\theta_\mu|$ as 0.013. However, in this scenario, the contribution to the electron EDM d_e , is significantly enhanced, with electron EDM d_e exceeding the corresponding upper bound by several orders of magnitude. Therefore, to satisfy the current experimental upper limits, we require contributions from different CPV terms to cancel each other out. Subsequently, we set other CPV phases to zero to explore the cancellation between θ_μ and θ_{M_2} . We perform a scan over the parameter space $[\theta_\mu = (-\pi, \pi), \theta_{M_2} = (-\pi, \pi)]$ while maintaining $|d_e| < 4.1 \times 10^{-30}$. The numerical results are shown in Fig. 11 (a). Furthermore, θ_{T_0} can also make a significant contribution to the Y_B , hence it is interesting to explore how θ_{T_0} affects d_e . Due to the suppression of the impact of θ_{T_0} by the smaller Y_e , it is not necessary to counteract the contribution of θ_{T_0} to d_e . Subsequently, in Fig. 11(b), we plot the relationship between d_e and θ_{T_0} , where the gray area represents the experimental upper limit for d_e , and the solid, dotted, and dashed lines correspond to $T_0 = 0.1$ TeV, 0.3 TeV, 0.5 TeV, respectively.

From the figure, it can be observed that when θ_μ is confined to a small phase space, the contributions from θ_μ and θ_{M_2} cancel each other out, which also indicates the contributions of θ_μ and θ_{M_2} are comparable, since θ_μ is the primary source of baryon asymmetry, concerns about whether the contribution to the electron EDM d_e from the large θ_μ values required for generating EWBG can be canceled can be relaxed. Furthermore, the contribution from

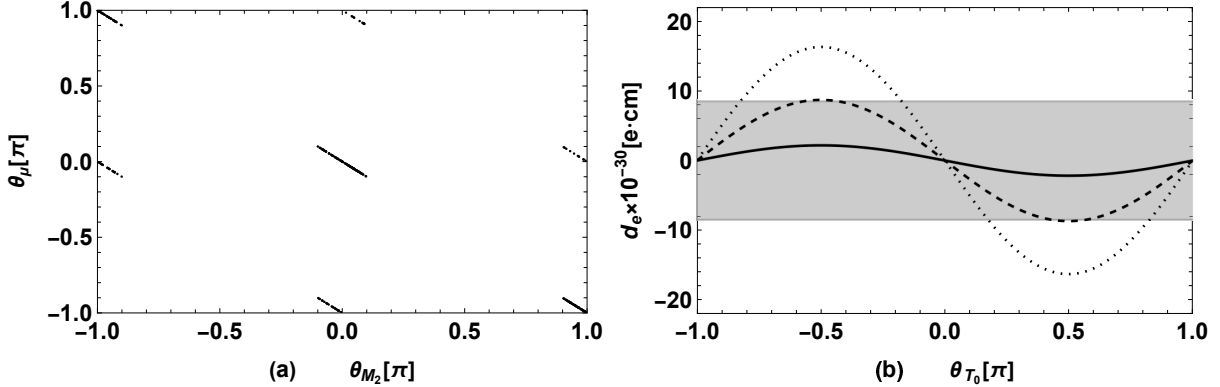


FIG. 11: Keeping $|d_e| < 4.1 \times 10^{-30}$, the cancellation between θ_μ and θ_{M_2} (a) are shown. And d_e versus θ_{T_0} are plotted for $T_0 = 0.1$ TeV (solid line), 0.3 TeV (dotted line), 0.5 TeV (dashed line), where the gray area denotes the present experimental upper bound on d_e .

θ_{T_0} is amplified by a large T_0 , while the contributions from θ_μ and θ_{M_2} are several orders of magnitude larger than that from θ_{T_0} . Therefore, it is hard for θ_{T_0} to cancel out the contribution from θ_μ (when θ_μ and θ_{T_0} are canceled out, the maximum value of θ_μ is $\mathcal{O}(10^{-3})$, which is insufficient to generate EWBG). This is in contrast to the situation in the MSSM [37], where when the contributions to the electron EDM d_e from θ_μ and θ_{T_0} cancel each other out, the maximum value of θ_μ can be large enough to induce EWBG. It can be seen that within our chosen parameter space, the contribution from the slepton is highly suppressed by the large slepton mass.

In the TNMSSM, the three new types of CPV phases, κ , χ_d and χ_u , also contribute to the electron EDM d_e . Among them, the contribution of κ is constrained by the coupling to singlet with smaller degree of freedom, and is insufficient to affect the final result of the EDM. Hence we do not delve into a detailed discussion of it here. To better elucidate the influence of parameters χ_d and χ_u on the electron EDM d_e , we have conducted separate graphical analyses for each parameter, with the results presented in Fig. 12, and Fig. 13, respectively.

Fig. 12 (a) depicts the parameter space scanned while holding all other CPV phases to zero and fixing χ_d at 0.01 (solid line), 0.02 (dashed line), 0.03 (dotted line), respectively, with the phase angle θ_{χ_d} varying from $-\pi$ to π . Fig. 12 (b) is keeping $|d_e| < 4.1 \times 10^{-30}$ and

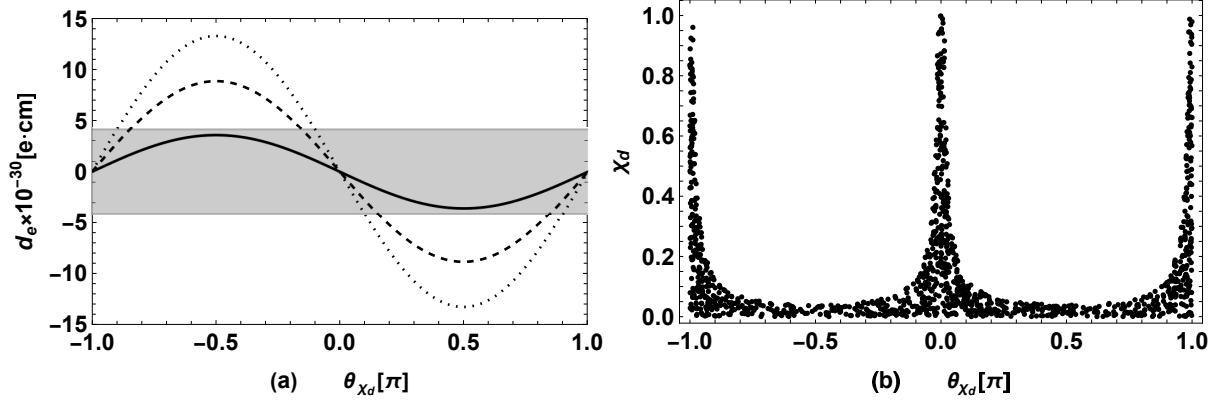


FIG. 12: χ_d effect on electron EDM d_e contribution. (a) is the curve drawn at different times of input χ_d , 0.01 (solid line), 0.02 (dashed line), 0.03 (dotted line). The shadow band is the experimental limit. And (b) is the distribution of the scanned phase space χ_d from 0 to 1 when $|d_e| < 4.1 \times 10^{-30}$ is maintained.

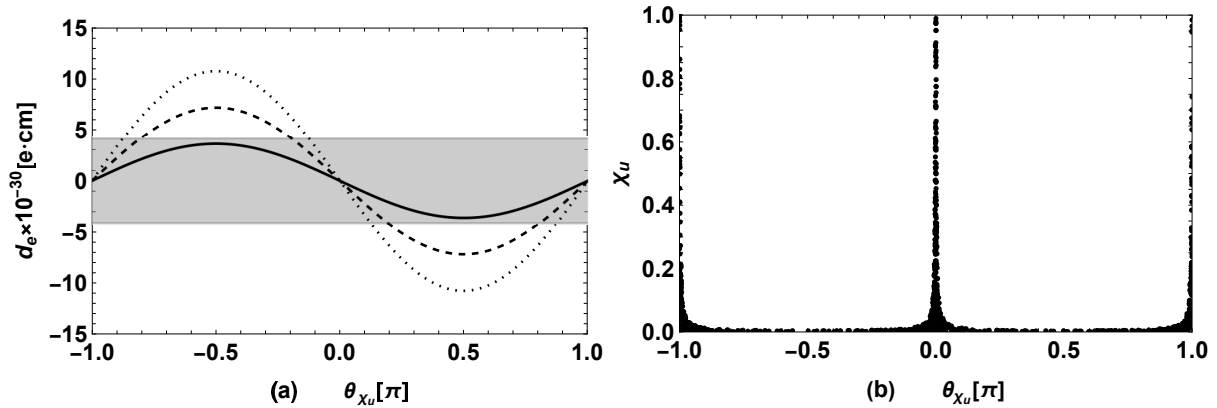


FIG. 13: χ_u effect on electron EDM d_e contribution. (a) is the curve drawn at different times of input χ_u , 0.001 (solid line), 0.002 (dashed line), 0.003 (dotted line). The shadow band is the experimental limit. And (b) is the distribution of the scanned phase space χ_u from 0 to 1 when $|d_e| < 4.1 \times 10^{-30}$ is maintained.

scan the regions of the parameter space $[\theta_{\chi_d} = (-\pi, \pi), \chi_d = (0, 1)]$. Fig. 13 (a) and (b) follow a similar approach, with the distinction that the parameter inputs related to χ_d have been replaced with those pertaining to χ_u . Fig. 12 (b) and Fig. 13 (b) reveal that the points

satisfying the experimental constraints for χ_d and χ_u form a narrow band at the base, with prominent peaks occurring near $\pm\pi$ and 0. This indicates that small values of χ_d and χ_u can satisfy the experimental constraints across the entire CPV phase space, whereas larger values of χ_d and χ_u only meet these constraints when $\sin\theta_{\chi_d}$ and $\sin\theta_{\chi_u}$ approach zero. This is also reflected in Fig. 12 (a) and Fig. 13 (a). The solid lines, representing smaller values of χ_d and χ_u , are observed to lie entirely within the shaded region, whereas the dashed and dotted lines, indicative of larger values of χ_d and χ_u , only fall within the shaded region near $\pm\pi$ and 0. Fig. 12 (b) and Fig. 13 (b) also reveal that when satisfying the experimental constraints, the band generated at the bottom of the phase space for χ_u is slightly lower than that for χ_d . This shows that the upper limit of χ_u satisfying the experimental limit in the entire phase space is less than the upper limit of χ_d . In other words, within the context of contributions to the electron EDM d_e , the parameter χ_u exhibits greater sensitivity compared to χ_d . This is also reflected in the relevant parameter input in Fig. 12 (a) and Fig. 13 (a), where the parameter input for χ_u is an order of magnitude smaller than that for χ_d .

V. SUMMARY

In this study, we focus on examining the impact of CPV sources on EWBG and the electron EDM d_e within the TNMSSM. Compared to the MSSM, the new triplet and singlet states mix with the MSSM doublet states at the tree level, and under such circumstances, a strong one-step PT can be realized. When resonance enhancement occurs, generating EWBG requires $|\theta_\mu| \gtrsim 0.013$, which makes significant contributions to the electron EDM. In this case, the cancellation effect is necessary to satisfy the experimental upper bound on the electron EDM. It is found that the contributions from θ_{M_2} (M_2 is the chargino mass term) to the electron EDM can cancel the ones from large θ_μ required by generating EWBG. When θ_μ and θ_{M_2} cancel each other out, θ_μ will be confined to a small phase space by the experimental bound on the electron EDM. Besides the traditional CPV sources μ and M_2 in SUSY models, the new CPV sources χ_u , χ_d , and κ can also make contributions to the electron EDM d_e , where χ_u and χ_d affect the theoretical prediction on d_e acutely, while the effects of κ is mild. This indicates that the cancellation phase between θ_μ and θ_{M_2} , which is

constrained to a small phase space, can be relaxed slightly by considering the effects of χ_u and χ_d .

Acknowledgments

The work has been supported by the National Natural Science Foundation of China (NNSFC) with Grants No. 12075074, No. 12235008, Hebei Natural Science Foundation with Grant No. A2022201017, No. A2023201041, the youth top-notch talent support program of the Hebei Province.

Appendix A: A simple derivation of the baryon-to-entropy density ratio Y_B .

Here, we briefly introduce Eq. (22) from Ref. [13].

First, the baryon-to-entropy density ratio can be expressed as

$$Y_B \equiv \frac{\rho_B}{s} , \quad (\text{A1})$$

where s represents the baryon entropy density at the time of electroweak phase transition

$$s = (2\pi^2)/45 \times g_{\text{eff}}(T) , \quad (\text{A2})$$

ρ_B is the baryon density

$$\rho_B = \frac{n_F}{2} \mathcal{A} \left[r_1 \Gamma_{\text{ws}} + r_2 \frac{\Gamma_{\text{ws}} v_w^2}{\Gamma_{\text{ss}} \bar{D}} \left(1 - \frac{D_q}{\bar{D}} \right) \right] \frac{\bar{D}}{v_w^2 + \mathcal{R}(\bar{D} + D_q)} , \quad (\text{A3})$$

n_F is the number of fermion families, v_w is the wall velocity, \bar{D} is an effective diffusion constant, D_q is the quark diffusion constant. $\Gamma_{\text{ws}}, \Gamma_{\text{ss}}$ can be written as respectively

$$\begin{aligned} \Gamma_{\text{ws}} &= 6\kappa\alpha_w^5 T , \kappa \simeq 20 , \\ \Gamma_{\text{ss}} &= 6\kappa' \frac{8}{3} \alpha_s^4 T , \kappa' \sim \mathcal{O}(1) , \end{aligned} \quad (\text{A4})$$

α_w and α_s are the weak and strong fine-structure constants, respectively.

r_1 and r_2 are related combinations of the statistical factors k_i

$$\begin{aligned} r_1 &= \frac{9k_Q k_T - 5k_Q k_B - 8k_T k_B}{k_H(9k_Q + 9k_T + k_B)} , \\ r_2 &= \frac{k_B^2(5k_Q + 4k_T)(k_Q + 2k_T)}{k_H(9k_Q + 9k_T + k_B)^2} , \end{aligned} \quad (\text{A5})$$

with

$$k_i(m_i/T) = k_i(0) \frac{c_{F,B}}{\pi^2} \int_{m/T}^{\infty} dx x \frac{e^x}{(e^x \pm 1)^2} \sqrt{x^2 - m^2/T^2}, \quad (\text{A6})$$

where for fermions (bosons) $c_{F(B)} = 6$ (3). \mathcal{R} is the relaxation term

$$\mathcal{R} = \Gamma_{\text{ws}} \left[\frac{9}{4} \left(1 + \frac{n_{\text{sq}}}{6} \right)^{-1} + \frac{3}{2} \right], \quad (\text{A7})$$

where n_{sq} indicates the number of light squark flavors. In Eq. (A3), \mathcal{A} is a solution that satisfies the Higgs density equation. Higgs density equation can be written

$$\dot{H} - \bar{D} \nabla^2 H + \bar{\Gamma} H - \bar{S} = \mathcal{O}(\delta_{ss}, \delta_Y), \quad (\text{A8})$$

where $\bar{\Gamma}$ is an effective decay constant and \bar{S} is an effective source term. Ref. [13] provides constraints on Eq. (A8), which are

- To simplify the problem to a one-dimensional issue, neglect the curvature of the wall, where all relevant functions depend on the variable $\bar{z} = |x + v_w t|$. Thus, $\bar{z} < 0$ is associated with the unbroken phase, $\bar{z} > 0$ with the broken phase, and the boundary wall extends over $0 < \bar{z} < L_w$, where L_w is the wall thickness.

When $\bar{z} > 0$, the relaxation term $\bar{\Gamma}$ is non-zero and constant.

- For simplicity, assume that the source behavior typical of a simple step function: \bar{S} nonzero and constant for $0 < \bar{z} < L_w$.

Then, the solution to Eq. (A8) can be written as

$$H(\bar{z}) = \mathcal{A} e^{v_w \bar{z} / \bar{D}}, \quad (\text{A9})$$

with

$$\mathcal{A} = k_H L_w \sqrt{\frac{\bar{\Gamma}}{\bar{D}}} \frac{S_{\bar{H}}^{CP} + S_{\bar{t}}^{CP}}{\Gamma_h + \Gamma_m}, \quad (\text{A10})$$

$S_{\bar{H}}^{CP}$ and $S_{\bar{t}}^{CP}$ are respectively the Higgsino CP-violating source and the Quark CP-violating source.

Finally, by separating the contributions of the Higgsino CP-violating source and the Quark CP-violating source in Eq. (A3), we can obtain:

$$Y_B = F_1 \sin \theta_\mu + F_2 \sin(\theta_\mu + \theta_T). \quad (\text{A11})$$

The first term that contains F_1 stems from the Higgsino source, while the F_2 term arises from the squark source. And θ_μ and θ_T are the corresponding phases.

Appendix B: Constants $C_{abc}^{L,R}$ appeared in our calculation and Form factors.

1. Constants $C_{abc}^{L,R}$

$$C_{\bar{e}_i \bar{v}_k \bar{\chi}_j^-}^L = U_{j,2}^* \sum_{b=1}^3 Z_{kb}^{V,*} \sum_{a=1}^3 U_{R,ia}^{e,*} Y_{e,ab} ,$$

$$C_{\bar{e}_i \bar{v}_k \bar{\chi}_j^-}^R = -g_2 \sum_{a=1}^3 Z_{ka}^{V,*} U_{L,ia}^e V_{j1} , \quad (\text{B1})$$

$$C_{\bar{\chi}_j^+ \bar{v}_k^* e_j}^L = -g_2 V_{i1}^* \sum_{a=1}^3 U_{L,ja}^{e,*} Z_{ka}^V ,$$

$$C_{\bar{\chi}_j^+ \bar{v}_k^* e_j}^R = \sum_{b=1}^3 \sum_{a=1}^3 Y_{e,ab}^* U_{R,ja}^e Z_{kb}^V U_{i2} , \quad (\text{B2})$$

$$C_{\bar{\chi}_i^0 \bar{e}_k^* e_j}^L = \frac{1}{2} (-2N_{i3}^* \sum_{b=1}^3 U_{L,jb}^{e,*} \sum_{a=1}^3 Y_{e,ab} Z_{k3+a}^E + \sqrt{2}g_1 N_{i1}^* \sum_{a=1}^3 U_{L,ja}^{e,*} Z_{ka}^E + \sqrt{2}g_2 N_{i2}^* \sum_{a=1}^3 U_{L,ja}^{e,*} Z_{ka}^E) ,$$

$$C_{\bar{\chi}_i^0 \bar{e}_k^* e_j}^R = -\sqrt{2}g_1 \sum_{a=1}^3 Z_{k3+a}^E U_{R,ja}^e N_{i1} - \sum_{b=1}^3 \sum_{a=1}^3 Y_{e,ab}^* U_{R,ja}^e Z_{kb}^E N_{i3} , \quad (\text{B3})$$

$$C_{\bar{e}_i \bar{e}_k \bar{\chi}_j^0}^L = -2N_{j3}^* \sum_{b=1}^3 Z_{kb}^{E,*} \sum_{a=1}^3 U_{R,ia}^{e,*} Y_{e,ab} - \sqrt{2}g_1 N_{j1}^* \sum_{a=1}^3 Z_{k3+a}^{E,*} U_{R,ia}^{e,*} ,$$

$$C_{\bar{e}_i \bar{e}_k \bar{\chi}_j^0}^R = \frac{1}{2} (-2 \sum_{b=1}^3 \sum_{a=1}^3 Y_{e,ab}^{e,*} Z_{k3+a}^{E,*} U_{L,ib}^e N_{j3} + \sqrt{2} \sum_{a=1}^3 Z_{ka}^{E,*} U_{L,ia}^e (g_1 N_{j1} + g_2 N_{j2})) , \quad (\text{B4})$$

$$C_{\bar{g}_{\bar{q}_i} \bar{q}_j}^L = -\sqrt{2}g_3 Z_{i,j}^{\bar{q}} e^{i\theta_3} , \quad C_{\bar{g}_{\bar{q}_i} \bar{q}_j}^R = \sqrt{2}g_3 Z_{i,j+3}^{\bar{q}} e^{-i\theta_3} ,$$

$$C_{\bar{q}_j \bar{q}_i \bar{g}}^L = \sqrt{2}g_3 Z_{i,j+3}^{\bar{q}*} e^{i\theta_3} , \quad C_{\bar{q}_j \bar{q}_i \bar{g}}^R = -\sqrt{2}g_3 Z_{i,j}^{\bar{q}*} e^{-i\theta_3} , \quad (\text{B5})$$

$$C_{\bar{\chi}_k^0 \bar{u}_i u_j}^L = -\frac{1}{6} \left(\sqrt{2} (g_1 Z_{k,1}^{N*} + 3g_2 Z_{k,2}^{N*}) Z_{i,j}^{\bar{u}} + 6Y_{u,j} Z_{k,4}^{N*} Z_{i,j+3}^{\bar{u}} \right) ,$$

$$C_{\bar{\chi}_k^0 \bar{u}_i u_j}^R = -\frac{1}{6} \left(\sqrt{2} (3g_2 Z_{k,2}^N + g_1 Z_{k,1}^N) Z_{i,j}^{\bar{u}*} + 6Y_{u,j}^* Z_{k,4}^N Z_{i,j+3}^{\bar{u}*} \right) , \quad (\text{B6})$$

$$C_{\bar{\chi}_k^0 \bar{d}_i d_j}^L = -\frac{1}{6} \left(\sqrt{2} (g_1 Z_{k,1}^{N*} - 3g_2 Z_{k,2}^{N*}) Z_{i,j}^{\bar{d}} + 6Y_{d,j} Z_{k,3}^{N*} Z_{i,j+3}^{\bar{d}} \right) ,$$

$$C_{\bar{\chi}_k^0 \bar{d}_i d_j}^R = -\frac{1}{6} \left(\sqrt{2} (-3g_2 Z_{k,2}^N + g_1 Z_{k,1}^N) Z_{i,j}^{\bar{d}*} + 6Y_{d,j}^* Z_{k,3}^N Z_{i,j+3}^{\bar{d}*} \right) , \quad (\text{B7})$$

$$C_{\bar{d}_j \bar{d} \bar{u}_i \bar{\chi}_k^-}^L = U_{k,2}^* \sum_{a=1}^3 Y_{d,a} Z_{a,j}^{CKM*} Z_{i,a}^{\bar{u}*} ,$$

$$C_{\bar{d}_j \bar{d} \bar{u}_i \bar{\chi}_k^-}^R = \sum_{a=1}^3 \left(-g_2 V_{k,1} Z_{a,j}^{CKM} Z_{i,a}^{\bar{u}*} + V_{k,2} Y_{u,a}^* Z_{a,j}^{CKM} Z_{i,a+3}^{\bar{u}*} \right) . \quad (\text{B8})$$

2. Form factors

Defining $x_i = \frac{m_i^2}{m_W^2}$, we can find the form factors:

$$\begin{aligned}
 I_1(x) &= \frac{1}{2(x-1)^2} \left(1 + x + \frac{2x}{x-1} \ln x \right) \\
 I_2(x) &= \frac{1}{6(x-1)^2} \left(10x - 26 - \frac{2x-18}{x-1} \ln x \right) \\
 I_3(x) &= \frac{1}{2(x-1)^2} \left(3 - x + \frac{2}{x-1} \ln x \right), \tag{B9}
 \end{aligned}$$

$$\begin{aligned}
 I_1(x_1, x_2) &= \frac{1}{16\pi^2} \left[\frac{1 + \ln x_2}{(x_2 - x_1)} + \frac{x_1 \ln x_1 - x_2 \ln x_2}{(x_2 - x_1)^2} \right] \\
 I_2(x_1, x_2) &= \frac{1}{16\pi^2} \left[-\frac{1 + \ln x_1}{(x_2 - x_1)} - \frac{x_1 \ln x_1 - x_2 \ln x_2}{(x_2 - x_1)^2} \right] \\
 I_3(x_1, x_2) &= \frac{1}{32\pi^2} \left[\frac{3 + 2 \ln x_2}{(x_2 - x_1)} - \frac{2x_2 + 4x_2 \ln x_2}{(x_2 - x_1)^2} - \frac{2x_1^2 \ln x_1}{(x_2 - x_1)^3} \right. \\
 &\quad \left. + \frac{2x_2^2 \ln x_2}{(x_2 - x_1)^3} \right] \\
 I_4(x_1, x_2) &= \frac{1}{96\pi^2} \left[\frac{11 + 6 \ln x_2}{(x_2 - x_1)} - \frac{15x_2 + 18x_2 \ln x_2}{(x_2 - x_1)^2} + \frac{6x_2^2 + 18x_2^2 \ln x_2}{(x_2 - x_1)^3} \right. \\
 &\quad \left. + \frac{6x_1^3 \ln x_1 - 6x_2^3 \ln x_2}{(x_2 - x_1)^4} \right], \tag{B10}
 \end{aligned}$$

$$J(x, y, z) = \ln x - \frac{y \ln y - z \ln z}{y - z}. \tag{B11}$$

- [1] R. Cooke, M. Pettini, R. A. Jorgenson, M. T. Murphy and C. C. Steidel, *Astrophys. J* **781**, 31 (2014).
- [2] P. A. R. Ade *et al.* [Planck Collaboration], *Astron. Astrophys* **594**, A13 (2016).
- [3] V. A. Kuzmin, V. A. Rubakov and M. E. Shaposhnikov, *Phys. Lett. B* **155**, 36 (1985).
- [4] M. B. Gavela, A. Le Yaouanc, L. Oliver, O. Pene, J. C. Raynal and T. N. Pham, *Phys. Lett. B* **109**, 215 (1982).
- [5] W. Bernreuther and M. Suzuki, *Rev. Mod. Phys* **63**, 313 (1991) Erratum: [*Rev. Mod. Phys* **64**, 633 (1992)].
- [6] M. Pospelov and A. Ritz, *Phys. Rev. D* **89**, 056006 (2014).

- [7] S. Navas et al. (Particle Data Group), Phys. Rev. D **110**, 030001 (2024).
- [8] T. S. Roussy et al, Science **381**, adg4084 (2023), arXiv:2212.11841 [physics.atom-ph].
- [9] M. Dine, P. Huet, R. L. Singleton, Jr and L. Susskind, Phys. Lett. B **257**, 351 (1991).
- [10] A. G. Cohen and A. E. Nelson, Phys. Lett. B **297**, 111 (1992).
- [11] P. Huet and A. E. Nelson, Phys. Rev. D **53**, 4578 (1996).
- [12] D. Chang, W. F. Chang and W. Y. Keung, Phys. Rev. D **66**, 116008 (2002).
- [13] C. Lee, V. Cirigliano and M. J. Ramsey-Musolf, Phys. Rev. D **71**, 075010 (2005).
- [14] T. Konstandin, T. Prokopec, M. G. Schmidt and M. Seco, Nucl. Phys. B **738**, 1 (2006).
- [15] D. J. H. Chung, B. Garbrecht, M. J. Ramsey-Musolf and S. Tulin, Phys. Rev. Lett. **102**, 061301 (2009).
- [16] D. J. H. Chung, B. Garbrecht, M. J. Ramsey-Musolf and S. Tulin, JHEP **0912**, 067 (2009).
- [17] D. J. H. Chung, B. Garbrecht, M. J. Ramsey-Musolf and S. Tulin, Phys. Rev. D **81**, 063506 (2010).
- [18] V. Cirigliano, Y. Li, S. Profumo and M. J. Ramsey-Musolf, JHEP **1001**, 002 (2010).
- [19] C. W. Chiang and E. Senaha, JHEP **1006**, 030 (2010).
- [20] D. E. Morrissey and M. J. Ramsey-Musolf, New J. Phys. **14**, 125003 (2012).
- [21] J. Kozaczuk, S. Profumo, M. J. Ramsey-Musolf and C. L. Wainwright, Phys. Rev. D **86**, 096001 (2012).
- [22] M. Pietroni, Nucl. Phys. B **402**, 27 (1993).
- [23] A. T. Davies, C. D. Froggatt and R. G. Moorhouse, Phys. Lett. B **372**, 88 (1996).
- [24] S. J. Huber and M. G. Schmidt, Nucl. Phys. B **606**, 183 (2001).
- [25] J. Kang, P. Langacker, T. j. Li and T. Liu, Phys. Rev. Lett. **94**, 061801 (2005).
- [26] S. J. Huber, T. Konstandin, T. Prokopec and M. G. Schmidt, Nucl. Phys. B **757**, 172 (2006).
- [27] P. Nath, Phys. Rev. Lett **66**, 2565 (1991).
- [28] Y. Kizukuri and N. Oshimo, Phys. Rev. D **46**, 3025 (1992).
- [29] T. Falk and K. A. Olive, Phys. Lett. B **375**, 196 (1996).
- [30] T. Falk and K. A. Olive, Phys. Lett. B **439**, 71 (1998).
- [31] M. Brhlik, G. J. Good and G. L. Kane, Phys. Rev. D **59**, 115004 (1999).
- [32] A. Bartl, T. Gajdosik, W. Porod, P. Stockinger and H. Stremnitzer, Phys. Rev. D **60**, 073003

- (1999).
- [33] S. Abel, S. Khalil and O. Lebedev, Nucl. Phys. B **606**, 151 (2001).
 - [34] V. D. Barger, T. Falk, T. Han, J. Jiang, T. Li and T. Plehn, Phys. Rev. D **64**, 056007 (2001) [hep-ph/0101106].
 - [35] K. A. Olive, M. Pospelov, A. Ritz and Y. Santoso, Phys. Rev. D **72**, 075001 (2005) [hep-ph/0506106].
 - [36] V. Cirigliano, S. Profumo and M. J. Ramsey-Musolf, JHEP **0607**, 002 (2006) [hep-ph/0603246].
 - [37] S. Yaser Ayazi and Y. Farzan, Phys. Rev. D **74**, 055008 (2006).
 - [38] J. Engel, M. J. Ramsey-Musolf and U. van Kolck, Prog. Part. Nucl. Phys. **71**, 21 (2013).
 - [39] T. Chupp, P. Fierlinger, M. Ramsey-Musolf and J. Singh, Rev. Mod. Phys. **91**, 015001 (2019).
 - [40] T. Ibrahim, P. Nath, Phys. Rev. D **58**, 111301 (1998), arXiv:hep-ph/9807501 [hep-ph]; Erratum: Phys. Rev. D **60**, 099902 (1999).
 - [41] M. Carena, M. Quiros, C. E. M. Wagner, Nucl. Phys. B **524**, 3-22 (1998), arXiv:hep-ph/9710401 [hep-ph].
 - [42] K. Agashe, A. Azatov, A. Katz, and D. Kim, Phys. Rev. D **84**, 115024 (2011).
 - [43] T. Basak and S. Mohanty, Phys. Rev. D **86**, 075031 (2012).
 - [44] T. Basak and S. Mohanty, JHEP **2013** (2013) 130, 1-17.
 - [45] W. Abdallah, A. Hammad, S. Khalil and S. Moretti, Phys. Rev. D **95**, 055019 (2017).
 - [46] A. Elsayed, S. Khalil and S. Moretti, Phys. Lett. B **715**, 208 (2012).
 - [47] G. Brooijmans et al. [arXiv:1203.1488 [hep-ph]].
 - [48] L. Basso and F. Staub, Phys. Rev. D **87**, 015011 (2013).
 - [49] L. Basso et al., Comput. Phys. Commun. **184**, 698 (2013).
 - [50] A. Elsayed, S. Khalil, S. Moretti and A. Moursy, Phys. Rev. D **87**, 053010 (2013).
 - [51] S. Khalil and S. Moretti, Rept. Prog. Phys. **80**, 036201 (2017).
 - [52] N.-Y. Zhu, H.-X. Chen, H.-C. Hu, Sci. Rep. **14**, 20542 (2024).
 - [53] Z.-Y. Zhang, J.-L. Yang, H.-B. Zhang, T.-F. Feng, Phys. Rev. D **110**, 015035 (2024), arXiv:2406.18323 [hep-ph].
 - [54] H.-C. Hu, Z.-Y. Zhang, N.-Y. Zhu, H.-X. Chen, Chin. Phys. C **48**, 093101 (2024),

- arXiv:2406.00946 [hep-ph].
- [55] H.-X. Chen, S.-K. Cui, N.-Y. Zhu, Z.-Y. Zhang, H.-C. Hu, *Chin. Phys. C* **48**, 053104 (2024), arXiv:2310.02531 [hep-ph].
- [56] P. Athron, Csaba Bal'azs, A. Fowlie, L. Morris, L. Wu, *Prog. Part. Nucl. Phys.* (2023), Elsevier.
- [57] C. E. M. Wagner, arXiv preprint arXiv:2311.06949 (2023).
- [58] D. E. Morrissey, M. J. Ramsey-Musolf, *New J. Phys.* **14**, 125003 (2012), IOP Publishing.
- [59] M. Trodden, *Rev. Mod. Phys.* **71**, 1463 (1999), APS.
- [60] D. Delepine, J. M. Gerard, R. Gonzalez Felipe and J. Weyers, *Phys. Lett. B* **386**, 183 (1996).
- [61] M. Carena, M. Quiros and C. E. M. Wagner, *Phys. Lett. B* **380**, 81 (1996).
- [62] J. R. Espinosa, *Nucl. Phys. B* **475**, 273 (1996).
- [63] M. Carena, M. Quiros and C. E. M. Wagner, *Nucl. Phys. B* **524**, 3 (1998).
- [64] S. J. Huber and M. G. Schmidt, *Eur. Phys. J. C* **10**, 473 (1999).
- [65] M. Carena, M. Quiros, M. Seco and C. E. M. Wagner, *Nucl. Phys. B* **650**, 24 (2003).
- [66] S. Profumo, M. J. Ramsey-Musolf and G. Shaughnessy, *JHEP* **0708**, 010 (2007).
- [67] M. Carena, G. Nardini, M. Quiros and C. E. M. Wagner, *Nucl. Phys. B* **812**, 243 (2009).
- [68] D. Curtin, P. Jaiswal and P. Meade, *JHEP* **1208**, 005 (2012).
- [69] K. Krizka, A. Kumar and D. E. Morrissey, *Phys. Rev. D* **87**, 095016 (2013).
- [70] H. H. Patel and M. J. Ramsey-Musolf, *JHEP* **1107**, 029 (2011).
- [71] J.-L. Yang, T.-F. Feng, H.-B. Zhang, *Eur. Phys. J. C* **80**, 210 (2020), Springer.
- [72] A. Riotto, *Phys. Rev. D* **58**, 095009 (1998), APS.
- [73] P. Huet, A. E. Nelson, *Phys. Rev. D* **53**, 4578 (1996), APS.
- [74] S. Akula, C. Balzs, L. Dunn and G. White, *JHEP* **1711**, 051 (2017).
- [75] K. Enqvist, A. Riotto, I. Vilja, *Phys. Lett. B* **438**, 273-280 (1998), Elsevier.
- [76] E. Braaten, R. D. Pisarski, *Phys. Rev. D* **46**, 1829 (1992), APS
- [77] T.-F. Feng, L. Sun and X.-Y. Yang, *Nucl. Phys. B* **800** (2008) 221 [arXiv:0805.1122].
- [78] T.-F. Feng, L. Sun and X.-Y. Yang, *Phys. Rev. D* **77** (2008) 116008 [arXiv:0805.0653].
- [79] T.-F. Feng and X.-Y. Yang, *Nucl. Phys. B* **814** (2009) 101 [arXiv:0901.1686].
- [80] H.-B. Zhang, T.-F. Feng, Z.-F. Ge, S.-M. Zhao, *JHEP* **02**, 012 (2014), arXiv:1401.2704 [hep-

- ph].
- [81] H. B. Zhang, T. F. Feng, S. M. Zhao and T. J. Gao, Nucl. Phys. B **873**, 300 (2013) [Erratum: Nucl. Phys. B **879**, 235 (2014)].
 - [82] H. B. Zhang, T. F. Feng, G. H. Luo, Z. F. Ge and S. M. Zhao, JHEP **1307**, 069 (2013) [Erratum: JHEP **1310**, 173 (2013)].
 - [83] X. Y. Yang and T. F. Feng, Phys. Lett. B **675**, 43 (2009).
 - [84] J. L. Yang, T. F. Feng, Y. L. Yan, W. Li, S. M. Zhao and H. B. Zhang, Phys. Rev. D **99**, 015002 (2019).
 - [85] M. Pospelov and A. Ritz, Phys. Rev. D **63**, 073015 (2001).
 - [86] E. Braaten, C. S. Li and T. C. Yuan, Phys. Rev. Lett. **64**, 1709 (1990).
 - [87] G. Degrassi, E. Franco, S. Marchetti and L. Silvestrini, JHEP **0511**, 044 (2005).
 - [88] F. Sala, JHEP **1403**, 061 (2014).
 - [89] T. F. Feng, X. Q. Li, J. Maalampi and X. M. Zhang, Phys. Rev. D **71**, 056005 (2005).
 - [90] G. F. Giudice and A. Romanino, Phys. Lett. B **634**, 307 (2006).
 - [91] L. Alvarez-Gaume, J. Polchinski and M. B. Wise, Nucl. Phys. B **221**, 495 (1983).
 - [92] A. Strumia, Nucl. Phys. B **482**, 24 (1996).
 - [93] S. Profumo, M. J. Ramsey-Musolf and S. Tulin, Phys. Rev. D **75**, 075017 (2007).
 - [94] Z. J. Yang, J. L. Yang, S. M. Zhao, X. G. Wu and T. F. Feng, Eur. Phys. J. C **84**, 1216 (2024).
 - [95] M. Carena, M. Quiros, A. Riotto, I. Vilja and C. E. M. Wagner, Nucl. Phys. B **503**, 387 (1997).